applied sciences

MDPI

Article

Modeling and Verification of Electromagnetic-Thermal Coupling for Electromagnetic Track Launch Considering the Dynamic Conductivity

Rongge Yan [1,2,*], Jinbo Jiang [1,2], Qingxin Yang [1,2] and Kang An [1,2]

[1] State Key Laboratory of Reliability and Intelligence of Electrical Equipment, Hebei University of Technology, Tianjin 300401, China; 202121401046@stu.hebut.edu.cn (J.J.); qxyang@tjut.edu.cn (Q.Y.); 202121401110@stu.hebut.edu.cn (K.A.)
[2] Key Lab of Electromagnetic Field and Electrical Apparatus Reliability of Hebei Province, Hebei University of Technology, Tianjin 300401, China
* Correspondence: yanrg@hebut.edu.cn; Tel.: +86-13642116378

Abstract: In order to solve the problems of insufficient precision of the armature velocity and inductance gradient in the process of finite element calculation of the electromagnetic track launcher, an improved dynamic conductivity electromagnetic-thermal coupling model is proposed to make the calculated results closer to the actual working condition. Firstly, the finite element analysis for the electromagnetic-thermal field is carried out. Then, considering the influence of dynamic conductivity on the armature velocity and inductance gradient, an improved dynamic conductivity electromagnetic-thermal coupling model based on finite element analysis is established, whose parameters are identified by the proposed PSO-GA hybrid algorithm. Moreover, the predicted values of armature velocity and inductance gradient are also obtained. Finally, the experimental platform of the electromagnetic track launcher is built to verify the improved model. By comparing the predicted value of the improved model with the experimental test value, it is found that the improved model can further reduce the calculated error from 5.79% to 1.18%, which provides a certain theoretical basis for the full true simulation of the electromagnetic track launch.

Keywords: electromagnetic track launch; electromagnetic-thermal coupling; armature and track dynamic conductivity; dynamic inductance gradient

check for updates

Citation: Yan, R.; Jiang, J.; Yang, Q.; An, K. Modeling and Verification of Electromagnetic-Thermal Coupling for Electromagnetic Track Launch Considering the Dynamic Conductivity. *Appl. Sci.* **2023**, *13*, 8739. https://doi.org/10.3390/app13158739

Received: 29 June 2023
Revised: 25 July 2023
Accepted: 27 July 2023
Published: 28 July 2023

Copyright: © 2023 by the authors. Licensee MDPI, Basel, Switzerland. This article is an open access article distributed under the terms and conditions of the Creative Commons Attribution (CC BY) license (https://creativecommons.org/licenses/by/4.0/).

1. Introduction

Electromagnetic launch technology is a new concept for an acceleration method that has been rapidly developed in recent years. Due to the technical advantages of fast speed, high efficiency, rapid start and good reliability, it has a wide application prospect in both military and civil fields [1,2]. Electromagnetic launch technology can be divided into the electromagnetic ejection technology, electromagnetic pushing technology and electromagnetic track launch technology according to the launch length and acceleration degree [3]. So far, the electromagnetic track launch technology is regarded as one of the effective means to enhance the tactical combat capability of conventional weapons in the future. Owing to good development prospects and technical advantages, it is an important research direction in the field of electromagnetic launch. An electromagnetic track launcher can increase the armature to a high speed within tens of milliseconds, which leads to a relatively complex experimental environment, and the research is relatively dependent on numerical simulation calculation [4–7]. Therefore, in order to achieve further popularization and application, how to improve the calculated accuracy of the simulation model and achieve full true simulation calculation is the key issue to be solved at present.

In the actual working process of the electromagnetic track launcher, extreme conditions such as high frequency, high current and the high temperature rise gradient generated will

lead to distortion of material parameters rather than maintaining a constant. The influence of dynamic parameters on the launcher cannot be ignored. Therefore, it is necessary to comprehensively consider the output under the influence of dynamic parameters so as to make it closer to the actual launch condition.

On the dynamic parameters of the electromagnetic track launcher, a lot of research in related fields has been carried out. Because the calculated equation of the armature electromagnetic force is directly related to the inductance gradient, the current research mainly focuses on the calculation of the dynamic inductance gradient. In the early studies, Batteh et al. [8,9] suggest that the inductance gradient is only related to the track size. When the track size is unchanged, the inductance gradient is also unchanged. Yang et al. [10] analyze the distribution of the inductance gradient with current frequency. Zhai et al. [11] consider the velocity skin effect and calculated the dynamic inductance gradient by introducing a velocity frequency. Peng et al. [12] propose an analytical calculated method for the inductance gradient which comprehensively considers the influence of the guide track size and current diffusion. However, in the actual working process, the temperature of the launcher will rise rapidly due to high frequency and high current. Under the influence of high temperature and high temperature rise gradient, the conductivities of the armature and track will undergo an enormous change, which will have an impact on the armature velocity and inductance gradient. The above references have carried out sufficient theoretical analysis on the electromagnetic track launcher, but do not consider the influence of high temperature on the conductivity of the launcher. Wang et al. [13] give the inductance gradient with different conductivities, but do not consider the influence of the dynamic conductivity on the inductance gradient.

There are few studies on dynamic conductivity in recent years, therefore, this paper firstly analyzes the correlation among the physical quantities such as temperature, conductivity, armature velocity and inductance gradient by using the finite element method, and the improved model of dynamic conductivity electromagnetic-thermal coupling is established on this basis. Then, improved model parameters are identified by using the proposed PSO-GA hybrid algorithm, and the predicted values of armature velocity and inductance gradient considering the influence of dynamic conductivity are obtained. Finally, the experiment platform of the electromagnetic track launcher is built to verify the improved model. It is found that the improved model can further reduce the calculated error, which provides a reference for the full true simulation of electromagnetic track launch.

2. Finite Element Analysis of the Electromagnetic Track Launcher

2.1. Finite Element Analysis Method

2.1.1. Governing Equation

The electromagnetic launch process can be regarded as a solution problem of a three-dimensional transient eddy current field containing a moving conductor. The electromagnetic track launcher can be divided into two areas: armature and track. The track is divided into the inner track and outer track, which are parallel to each other. The armature contacts with the inner track. When the launcher is working, the excitation current flows in from the upper outer track and out from the lower inner track through the armature. An electromagnetic thrust is generated and pushes the armature to launch out. The schematic diagram of electromagnetic track launcher is shown in Figure 1, where Figure 1a is the side view of the launcher and (b) the front one. I the excitation current, v the armature velocity and the other model parameters in Figure 1 are shown in Table 1.

Since it is not convenient to solve Maxwell's equations directly, electromagnetic potentials are usually introduced during finite element calculation to simplify the problem, of which the $\boldsymbol{A}$-φ method is a commonly used expression, which expresses the electromagnetic field governing equations through the magnetic vector potential $\boldsymbol{A}$ and the electric scalar potentials φ, making their numerical calculations easier to realize [14].

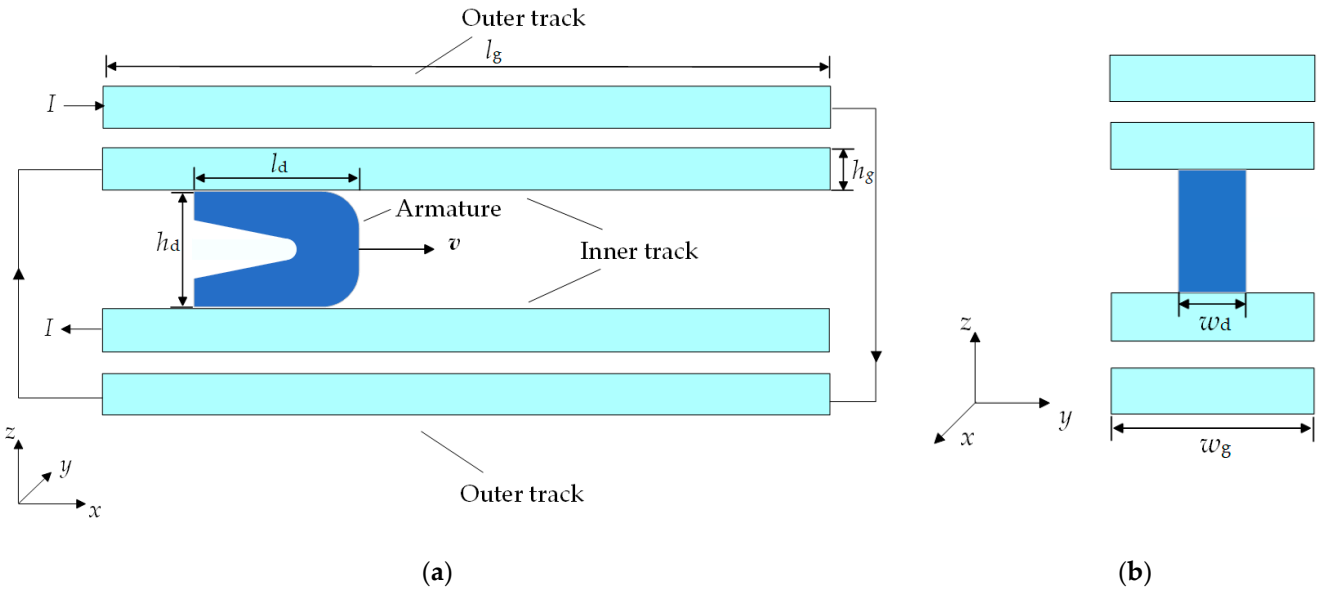


Figure 1. Schematic diagram of electromagnetic track launcher. (**a**) Side view of the launcher; (**b**) front view of the launcher.

Table 1. The model parameters of the electromagnetic track launcher.

Model Parameters	Symbol	Values
Armature length/(mm)	l_d	26.82
Armature height/(mm)	h_d	17.88
Armature width/(mm)	w_d	9.9
Track length/(mm)	l_g	203
Track height/(mm)	h_g	2
Track width/(mm)	w_g	30

Ignoring the displacement current, the diffusion equations of armature and track can be deduced by using the A-φ method as follows:

$$\begin{cases} \nabla^2 \boldsymbol{A} - \mu_d \sigma_d (\nabla \varphi + \frac{\partial \boldsymbol{A}}{\partial t} - v \times \nabla \times \boldsymbol{A}) = \boldsymbol{0} \\ \nabla^2 \boldsymbol{A} - \mu_g \sigma_g (\nabla \varphi + \frac{\partial \boldsymbol{A}}{\partial t}) = \boldsymbol{0} \end{cases} \tag{1}$$

where, μ_d, μ_g represent the armature permeability and the track one, respectively. σ_d, σ_g represent the armature conductivity and the track one, respectively.

When the launcher is working, the magnetic induction intensities cancel each other out in the direction z and there is only a component in the direction y, so $\boldsymbol{A}$ has components only in the directions x, z and v only in the direction x. Therefore, ignoring $\frac{\partial A_x}{\partial y}$, $\frac{\partial A_z}{\partial y}$, A_y, v_y and v_z, Equation (1) is written as follows [11]:

$$\begin{cases} \frac{\partial^2 A_x}{\partial x^2} + \frac{\partial^2 A_x}{\partial z^2} - \mu_d \sigma_d \left(\frac{\partial \varphi}{\partial x} + \frac{\partial A_x}{\partial t} \right) = 0 \\ \frac{\partial^2 A_z}{\partial x^2} + \frac{\partial^2 A_z}{\partial z^2} - \mu_d \sigma_d \left[\frac{\partial \varphi}{\partial z} + \frac{\partial A_z}{\partial t} - v_x \left(\frac{\partial A_x}{\partial z} - \frac{\partial A_z}{\partial x} \right) \right] = 0 \\ \frac{\partial^2 A_x}{\partial x^2} + \frac{\partial^2 A_x}{\partial z^2} - \mu_g \sigma_g \left(\frac{\partial \varphi}{\partial x} + \frac{\partial A_x}{\partial t} \right) = 0 \\ \frac{\partial^2 A_z}{\partial x^2} + \frac{\partial^2 A_z}{\partial z^2} - \mu_g \sigma_g \left(\frac{\partial \varphi}{\partial z} + \frac{\partial A_z}{\partial t} \right) = 0 \end{cases} \tag{2}$$

During the working process of the launcher, the track surface temperature changes rapidly, in which the heat conduction process causes the greatest impact. By consider-

ing the heat conduction process only, the track heat transfer governing equation is as follows [15,16]:

$$\rho c \frac{\partial \boldsymbol{T}}{\partial t} = \nabla \cdot (k \nabla \boldsymbol{T}) + Q_1 + Q_2 + Q_3 \tag{3}$$

where, ρ is the material density of launcher, c the specific heat capacity of material, λ the thermal conductivity, Q_1 the heating of the track resistance, Q_2 the heating of the contact resistance and Q_3 the friction heat generation between the armature and track.

2.1.2. Mesh Analysis and Discretization

According to the armature and track divided, the boundary conditions in the computational domain can be given, which mainly consist of the armature-track contact surface condition, the track-air domain interface condition and the armature-air domain interface condition, as shown below:

$$\begin{cases} \boldsymbol{n}_{ij} \times \left(\boldsymbol{E}_i - \boldsymbol{E}_j\right) = \boldsymbol{0} \\ \boldsymbol{n}_{ij} \times \left(\boldsymbol{H}_i - \boldsymbol{H}_j\right) = \boldsymbol{0} \\ \boldsymbol{n}_{ij} \times \left(\boldsymbol{D}_i - \boldsymbol{D}_j\right) = \boldsymbol{0} \\ \boldsymbol{n}_{ij} \times \left(\boldsymbol{B}_i - \boldsymbol{B}_j\right) = \boldsymbol{0} \end{cases} \tag{4}$$

where, $\boldsymbol{n}_{ij}$ is the normal vector of the manifold. Where $i = 1$, $j = 2$, $\boldsymbol{n}_{ij}$ represents the armature-track contact surface condition, $i = 1$, $j = 3$ represents the track-air domain interface condition and $i = 2$, $j = 3$ represents the armature-air domain interface condition.

The finite element calculation includes spatial discretization and time discretization. Firstly, Equation (2) is spatially discretized, and the solution region is dissected into grids, the result of grid segmentation is shown in Figure 2.

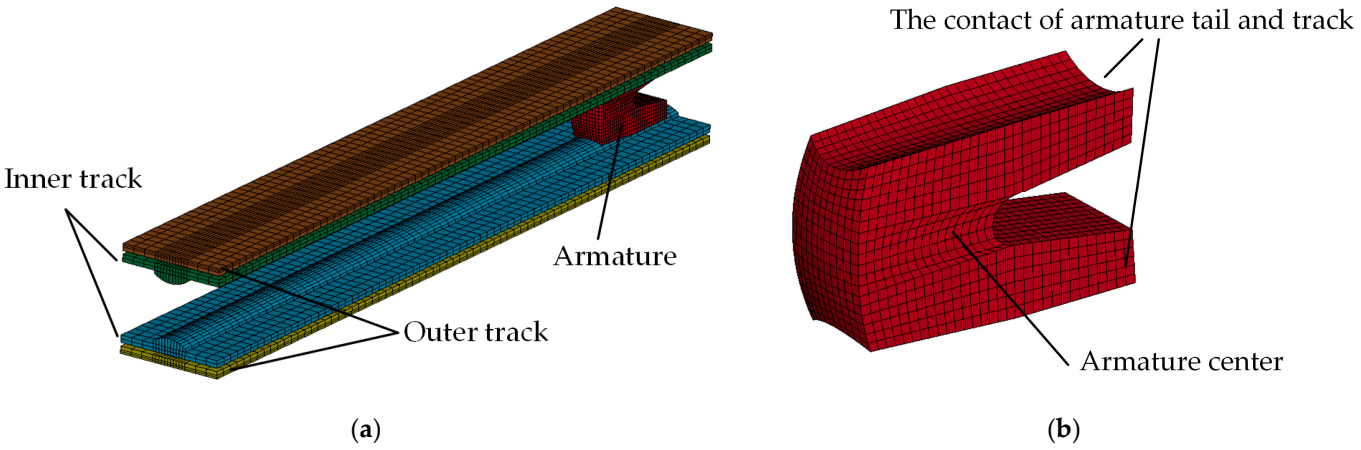


Figure 2. Grid segmentation of electromagnetic track launcher. (**a**) Armature, inner and outer tracks of the launcher; (**b**) armature center and the contact of the armature tail and track.

Then, the discretization of the dissected cells is substituted into the governing equations, and the final form of the matrix equation is obtained as [17]:

$$\boldsymbol{K}\boldsymbol{U} + \boldsymbol{M}\frac{\partial \boldsymbol{U}}{\partial t} = \boldsymbol{F} \tag{5}$$

where $\boldsymbol{K}$, $\boldsymbol{M}$ and $\boldsymbol{F}$ are the overall stiffness matrix, overall mass matrix and overall load vector, respectively. $\boldsymbol{U}$ is the overall unknown function vector.

Then, the time discretization of the above equation is obtained by using the Euler difference equation.

$$\boldsymbol{K}\boldsymbol{U}^{t+\Delta t} + \frac{\boldsymbol{M}\left(\boldsymbol{U}^{t+\Delta t} - \boldsymbol{U}^{t}\right)}{\Delta t} = \boldsymbol{F}^{t+\Delta t} \tag{6}$$

where, Δt is the time step.

By solving the system of algebraic equations formed by the above discretization, the distribution of the current, magnetic and temperature fields in the solution region of the launcher can be obtained.

The magnetic induction intensity and electric field intensities are:

$$\begin{cases} \boldsymbol{B} = \nabla \times \boldsymbol{A} \\ \boldsymbol{E} = -\left(\frac{\partial \boldsymbol{A}}{\partial t} + \nabla \varphi\right) \end{cases} \tag{7}$$

The armature electromagnetic thrust density is:

$$f_e = \boldsymbol{J} \times \boldsymbol{B} \tag{8}$$

2.2. Finite Element Calculation Results

2.2.1. Armature Velocity

The excitation current obtained by fitting the experimental current is used in the finite element calculation in this paper, which is basically consistent with the experimental current, and more accurate calculated results can be obtained. The expression of excitation current is as follows:

$$I = \begin{cases} I_0 \sin(2.5\pi t) \; 0 \le t \le 0.2 \text{ ms} \\ I_0 \, e^{-0.61(t-0.2)} \quad 0.2 < t \le 0.6 \text{ ms} \end{cases} \tag{9}$$

where, I_0 is the excitation current peak at 318 kA.

The curves of excitation current and experimental one are shown in Figure 3:

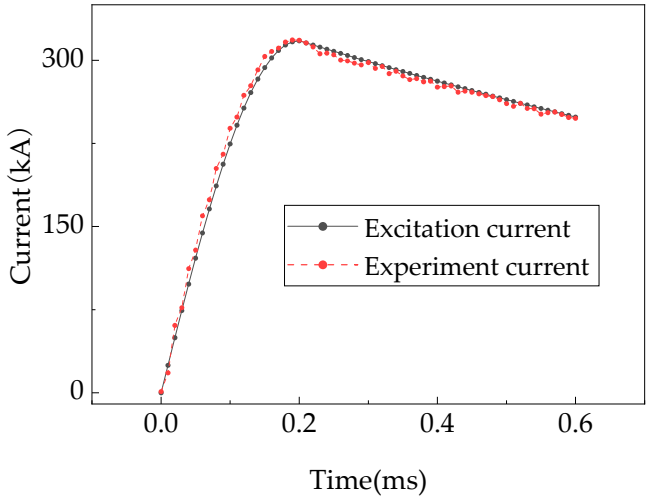


Figure 3. Curves of excitation current and experimental one.

In the actual launching process, the armature is subjected to three forces, including electromagnetic thrust, friction force and air resistance. According to the balance of forces, the resultant force of the armature should be:

$$F_a = F_e - f_1 v_{\text{af}}^2 - f_2 m_0 g \tag{10}$$

where, F_a is the resultant force of the armature, F_e the electromagnetic thrust of the armature, f_1 the wind resistance coefficient 7.9 $\times$ 10^{-5} kg/m, calculated by multiplying the coefficient of air resistance, air density and the windward area of the armature, v_{af} the armature velocity considering the influence of air resistance and friction force, f_2 the sliding friction coefficient which is generally 0.5, m_0 is the armature mass of 10 g, consistent with experimental armature mass. G is the acceleration due to gravity 9.8 m/s^2.

F_a can also be expressed by deriving v_{af}.

$$F_a = m_0 \frac{dv_{af}}{dt} \tag{11}$$

In summary, considering the influence of air resistance and the friction force, the driving equation of the armature is written as follows:

$$m_0 \frac{dv_{af}}{dt} = F_e - f v_{af}^2 - \mu_0 m_0 g \tag{12}$$

By solving Equation (12), v_{af} can be obtained as follows:

$$v_{af} = \sqrt{\frac{F_e - \mu_0 m_0 g}{f}} \cdot \left(\frac{e^{2t\frac{\sqrt{(F_e-\mu_0 m_0 g)f}}{m_0}} - 1}{e^{2t\frac{\sqrt{(F_e-\mu_0 m_0 g)f}}{m_0}} + 1} \right) \tag{13}$$

When the air resistance and friction force are far less than F_e, which means that $\frac{fv^2}{F_e} \to 0$, $\frac{\mu_0 m_0 g}{F_e} \to 0$, Equation (13) is changed as follows:

$$v_{af} = \frac{F_e}{m_0} t \tag{14}$$

According to the armature electromagnetic thrust calculated equation.

$$F_e = \frac{1}{2} L I^2 \tag{15}$$

where, L is the inductance gradient, typically between 0.8 μH/m and 1.2 μH/m.

It can be seen that when I reaches its peak value (318 kA), F_e can reach up to 5×10^4 N.

Because the air resistance and friction are very small compared with F_e, the influence can be ignored. The LS-dyna finite element software is used for simulation to obtain the armature velocity, as shown in Figure 4:

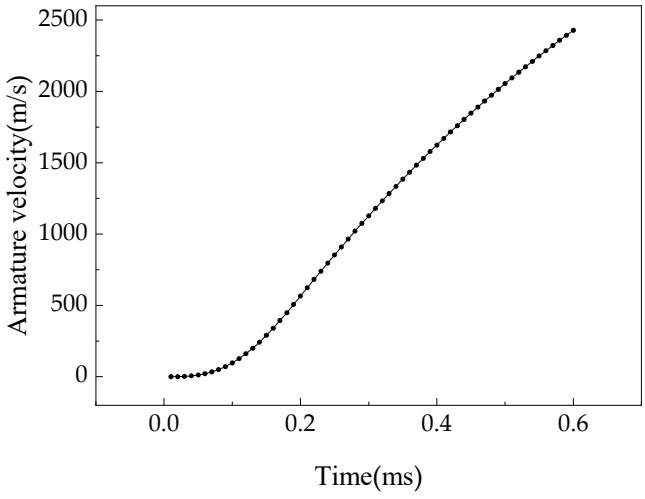


Figure 4. Finite element calculated value of armature velocity.

In order to provide data for the improved electromagnetic-thermal coupling model, multiple sets of finite element simulations are set up with the fixed track conductivity σ_g and the armature conductivity σ_d, fixed armature conductivities σ_d and track conductivities σ_g, respectively. The armature velocity calculated results are obtained and shown in Figure 5.

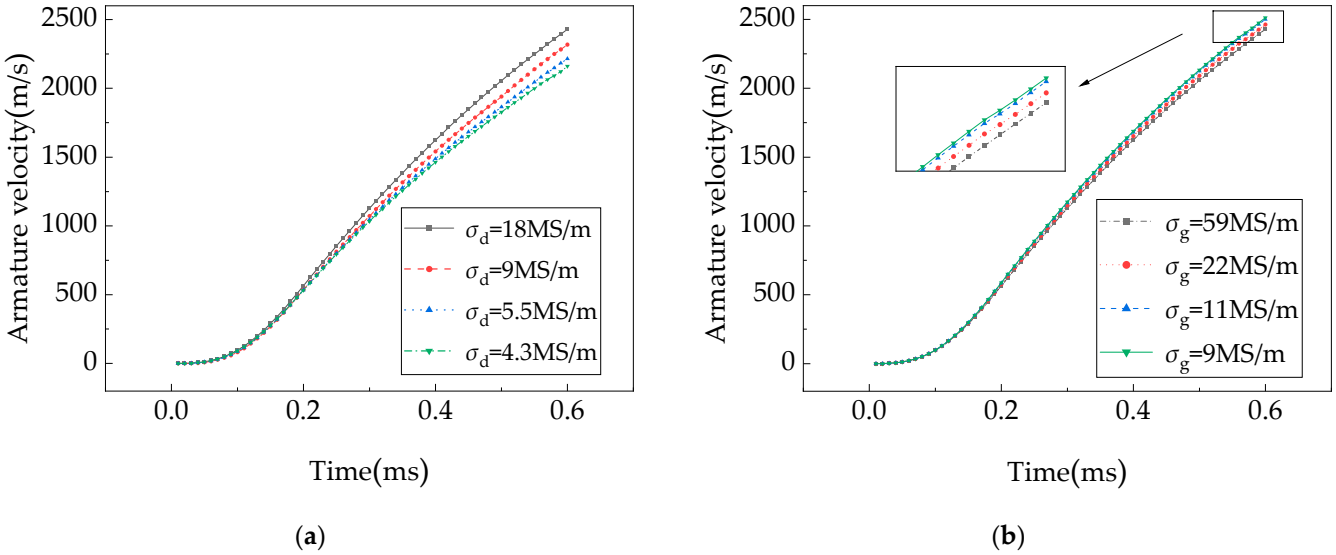


Figure 5. Curves of armature velocity with time at different conductivities. (**a**) Armature velocity at different armature conductivities σ_d; (**b**) armature velocity at different track conductivities σ_g.

It can be seen that, when the track conductivity σ_g is fixed, the armature velocity increases with the armature conductivity σ_d. This is due to the fact that the greater armature conductivity σ_d causes a more uniform the magnetic field distribution, and a larger armature electromagnetic thrust and velocity. Conversely, the armature velocity decreases with the increase of the track conductivity σ_g. This is due to the fact that the greater track conductivity σ_g increases the skin depth, which reduces the diffusion speed of the magnetic field in the track, and the rising speed of the armature electromagnetic thrust. Thus, the armature velocity decreases.

2.2.2. Inductive Gradient

The skin effect is a physical phenomenon that occurs in conductors in alternating electromagnetic fields. In the armature launching process, the state of motion of charge through the launcher changes due to the strong magnetic field, which causes the uneven distribution of the current density, and the inductance gradient is affected. The current density distributions at different time are calculated by LS-dyna as shown in Figure 6.

It can be seen that the current is mainly concentrated in the armature center and the contact of the armature tail and track due to the skin effect, rather than a uniform distribution, which causes the inductance gradient of the launcher to change dynamically with time.

The inductance gradient curve is calculated by LS-dyna as shown in Figure 7.

In the finite element simulation software, multiple sets of finite element simulations are set up with a fixed track conductivity σ_g and armature conductivity σ_d, and fixed armature conductivities σ_d and track conductivities σ_g. The inductance gradient calculated results are obtained and shown in Figure 8.

It can be seen that, when the track conductivity σ_g is fixed, the inductance gradient increases with the armature conductivity σ_d. This is due to the fact that the greater armature conductivity σ_d causes a more uniform magnetic field distribution, and a larger inductance gradient. Conversely, the inductance gradient decreases with the increase of the track conductivity σ_g. This is due to the fact that the greater track conductivity σ_g increases the skin depth, which reduces the diffusion speed of the magnetic field in the track. Thus, the inductance gradient decreases.

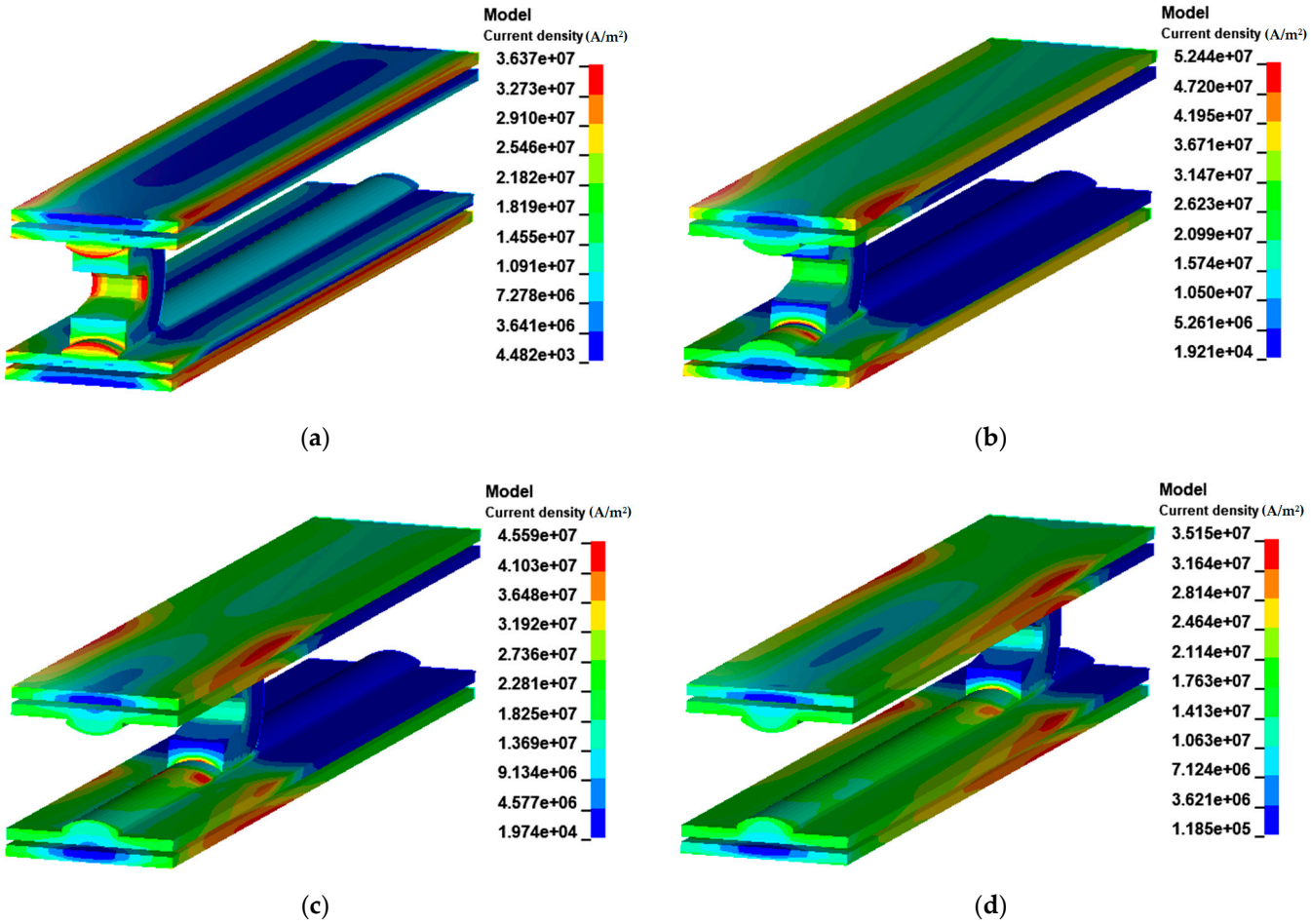


Figure 6. Current density distribution at different time points. (**a**) t = 0.10 ms; (**b**) t = 0.25 ms; (**c**) t = 0.40 ms; (**d**) t = 0.55 ms.

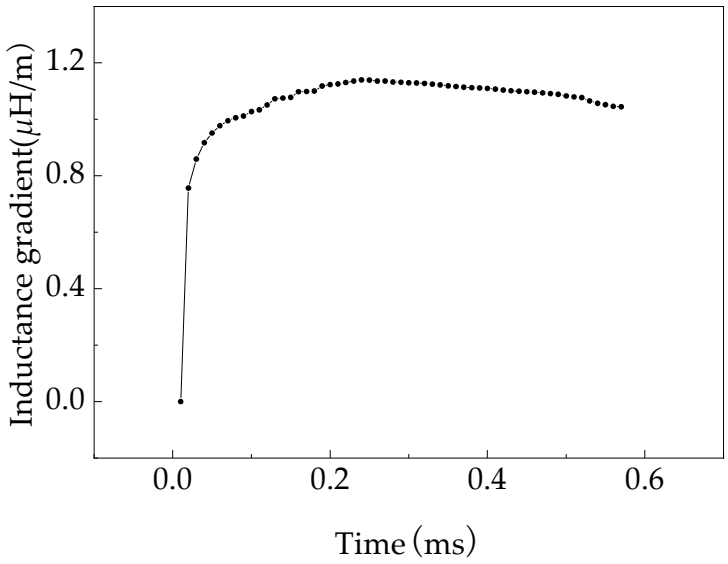


Figure 7. Inductance gradient curve with time.

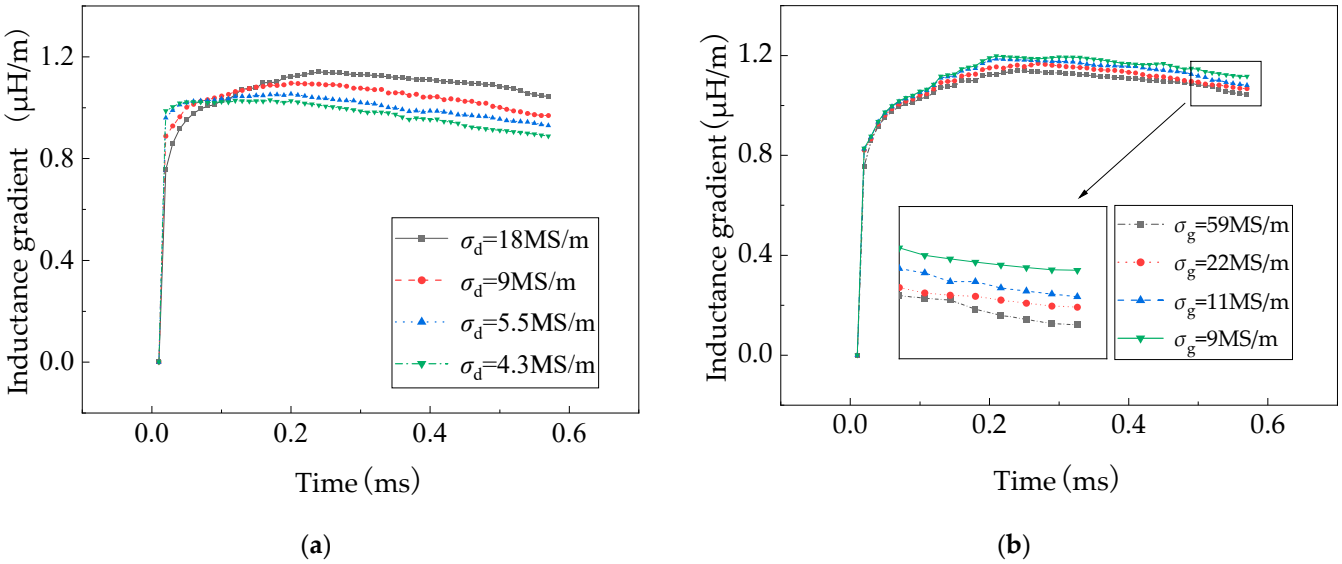


Figure 8. Inductance gradient curve with time at different conductivities. (**a**) Inductance gradient at different armature conductivities σ_d; (**b**) inductance gradient at different track conductivities σ_g.

2.2.3. Temperature of Armature and Track

In the armature launching process, the high frequency current will bring about a high temperature rise gradient. The temperature distributions at different times are calculated by LS-dyna as shown in Figure 9.

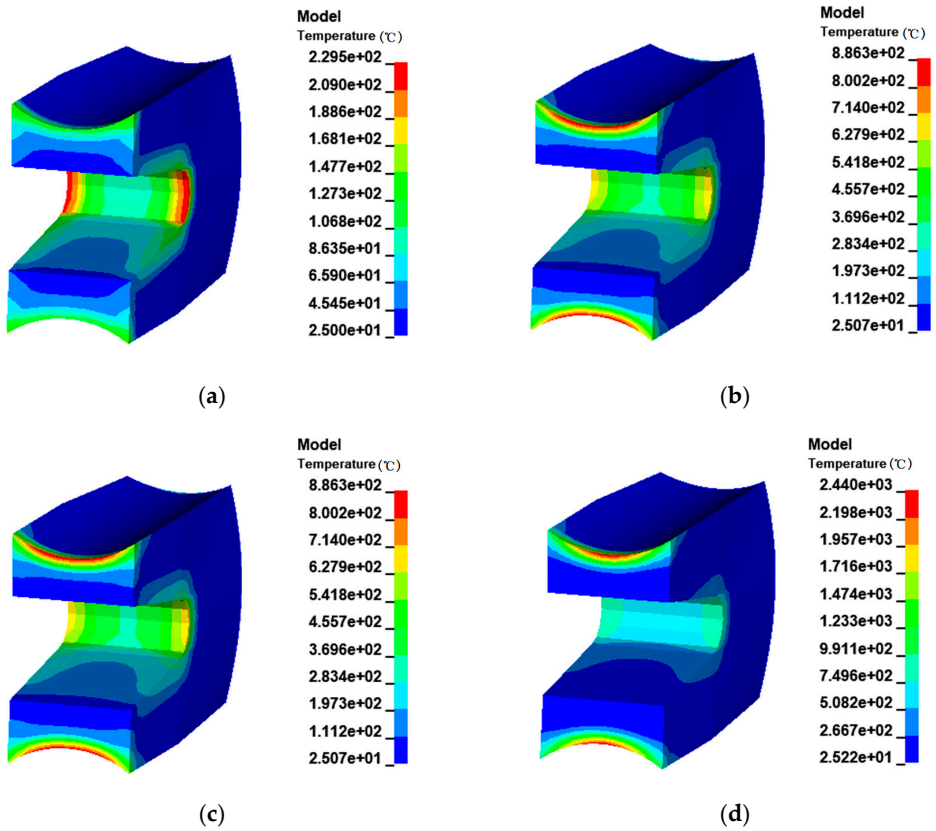


Figure 9. Temperature distribution at different time points. (**a**) t = 0.10 ms; (**b**) t = 0.25 ms; (**c**) t = 0.40 ms; (**d**) t = 0.55 ms.

It can be seen that the uneven distribution of the current density leads to a larger temperature of the armature at the current aggregation, and the heat is mainly concentrated in the armature center and the contact of the armature tail and track. This is consistent with the distribution of the current density in Figure 6.

The temperature curves of the armature and track are calculated by LS-dyna as shown in Figure 10.

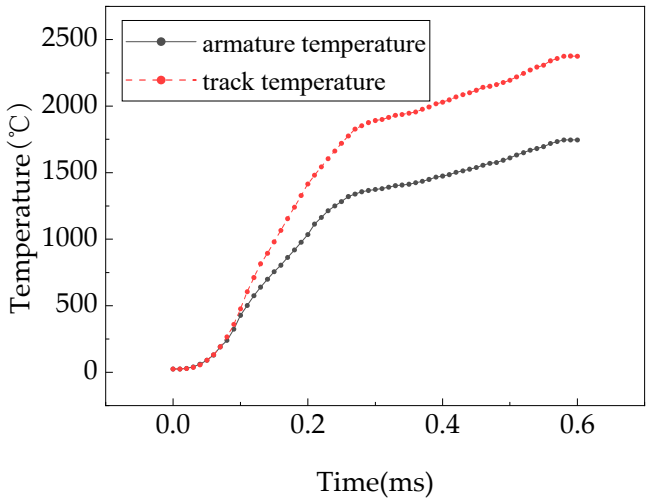


Figure 10. Temperature curves of the armature and track.

2.2.4. Conductivities of the Armature and Track

According to Figure 10, We can get:

$$\begin{cases} T_{\mathrm{d}} = T_{\mathrm{d}}(t) \\ T_{\mathrm{g}} = T_{\mathrm{g}}(t) \end{cases} \tag{16}$$

The relationships between the conductivities and temperature of the armature material and the track one are as follows:

$$\begin{cases} \sigma_{\mathrm{d}} = \sigma_{\mathrm{d}}(T_{\mathrm{d}}) \\ \sigma_{\mathrm{g}} = \sigma_{\mathrm{g}}(T_{\mathrm{g}}) \end{cases} \tag{17}$$

We can obtain the dynamic conductivity by considering Equations (16) and (17):

$$\begin{cases} \sigma_{\mathrm{d}} = \sigma_{\mathrm{d}}[T_{\mathrm{d}}(t)] \\ \sigma_{\mathrm{g}} = \sigma_{\mathrm{g}}[T_{\mathrm{g}}(t)] \end{cases} \tag{18}$$

3. Establishment of the Improved Electromagnetic-Thermal Coupling Model

In the available finite element calculation of the armature velocity and inductance gradient, the conductivities of the armature and track are usually considered as constant. However, in the actual launching process, the armature and track will produce a high temperature rise gradient due to the high frequency current, which causes the change of conductivity and affects the current diffusion, the armature velocity and the inductance gradient. In summary, this paper establishes an improved model by using a parameter identification method. Firstly, multi-group calculations of the armature velocity and inductance gradient are carried out by changing the conductivity values in the finite element analysis software Ls-dyna. Then, the prediction functions for the armature velocity and inductance gradient are obtained according to variation rules of the armature velocity and inductance gradient with conductivity values. Finally, the improved model of electromagnetic-thermal coupling is obtained by parameter identification. A flow chart of the establishment of the improved model is shown in Figure 11.

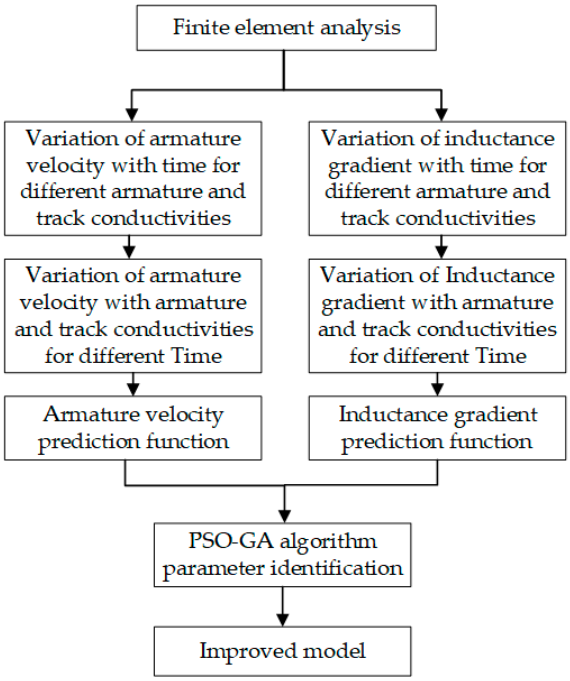


Figure 11. Flow chart of the establishment of the improved model.

3.1. Prediction Function of the Armature Velocity

Based on the data obtained from Figure 5, the armature velocity relations with the armature conductivity and track one at different times are obtained, which are shown in Figure 12.

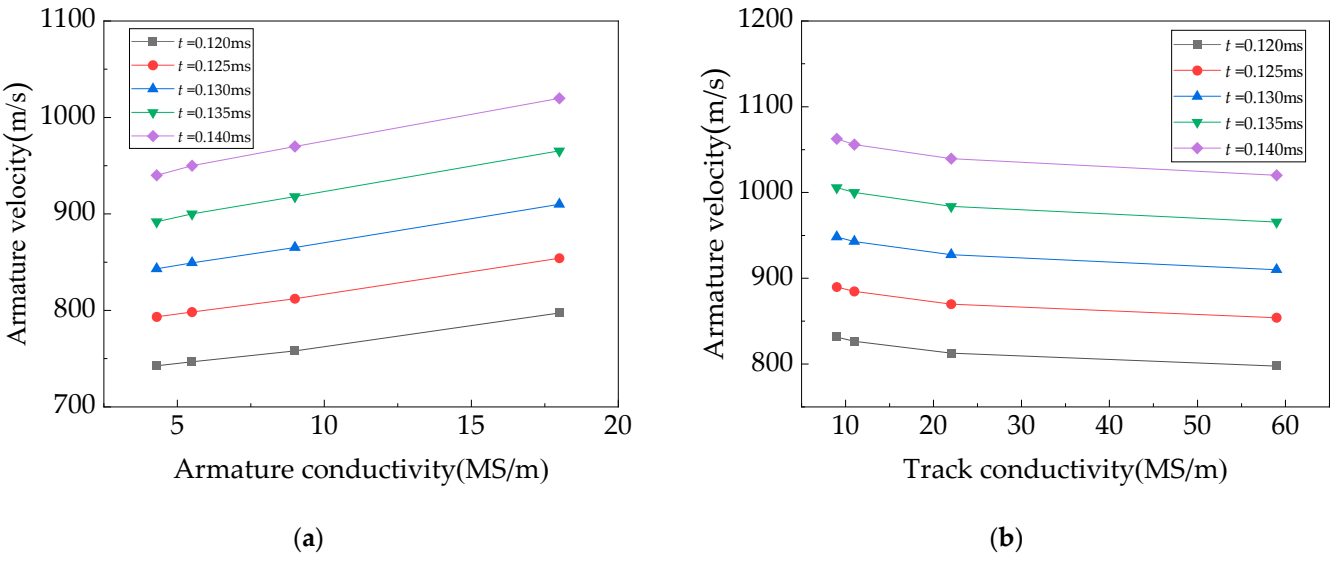


Figure 12. The armature velocity relations with the conductivity at different times. (**a**) Armature velocity curves with the armature conductivity σ_d; (**b**) armature velocity curves with the track conductivity σ_g.

It can be seen that, at the same time point, the armature velocity gradually increases with the armature conductivity σ_d, and gradually decreases with the track conductivity σ_g, in which the ascending (descending) speed gradually slows down. So, the following

equation can be used to approximately describe the armature velocity with the armature conductivity and track one.

$$\begin{cases} v_1 = r_1 \ln(\sigma_d) + s_1 \\ v_2 = r_2 \ln(\sigma_g) + s_2 \end{cases} \tag{19}$$

where, v_1 and v_2 are the influence factors of the armature velocity under the influence of the armature conductivity and the track one, respectively. σ_d and σ_g are the armature conductivity and the track one (MS/m), respectively. r_1, r_2, s_1 and s_2 are the corresponding fitting coefficients, respectively.

According to Equations (9), (11) and (15), the analytic armature velocity v_0 can be calculated by:

$$v_0 = \begin{cases} \frac{L_0 I_0^2}{m_0} \cdot \left[\frac{1}{4} t - \frac{1}{10\pi} \sin\left(\frac{\pi t}{0.2}\right) \right] & 0 \le t \le 0.2 \text{ ms} \\ \frac{L_0 I_0^2}{m_0} \cdot \left[\frac{1}{2.44} \left(1 - e^{-1.22(t-0.2)}\right) + 0.05 \right] & 0.2 < t \le 0.6 \text{ ms} \end{cases} \tag{20}$$

where, L_0 1.0 μH/m.

Then, the analytic relationship between the armature velocity v_0 and time is shown in Figure 13 [18].

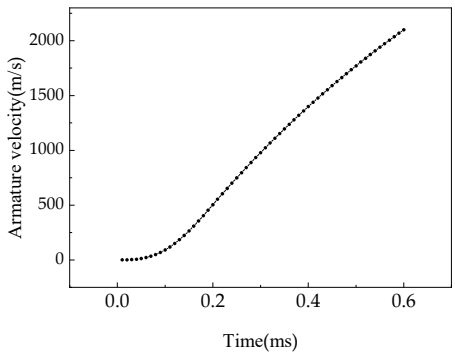


Figure 13. The analytic relationship between the armature velocity v_0 and time.

From Figures 5 and 13, it can be seen that, with the same conductivity, the finite element calculated value of the armature velocity is similar to the analytic value of the armature velocity. Therefore, the finite element calculated value of the armature velocity v can be represented by multiplying the analytic armature velocity v_0 by a coefficient k_0, i.e.,

$$v = k_0 v_0 \tag{21}$$

where k_0 can be obtained through interpolating the time and conductivity, which is shown in Figure 14.

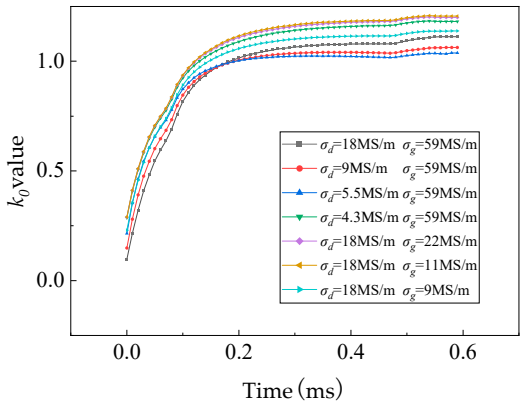


Figure 14. k_0 curves of time and conductivity.

It can be seen that k_0 changes dynamically with time with the same conductivity. The curves rise rapidly from 0 to 0.2 ms and gradually stabilize from 0.2 to 0.6 ms. Likewise, k_0 changes with the conductivity at the same time point. Therefore, when considering the dynamic conductivity, k_0 can be expressed as a multiplication of a function only related to time $k_0(t)$ and a function only related to conductivity (v_1 + v_2), i.e.,

$$k_0 = k_0(t) \cdot \left[r_1 \ln(\sigma_d) + r_2 \ln(\sigma_g) + s_0 \right] \tag{22}$$

where $s_0 = s_1 + s_2$.

Define $k_0(t)$ as follows:

$$k_0(t) = \sum_{i=0}^{n} w_i \, t^i \tag{23}$$

where w_i is the fitting coefficient, n is the degree of the fitting polynomial.

$k_0(t)$ is fitted by taking the average values of each group of curves in Figure 14 as the basis. The fitting coefficients are shown in Table 2. When n = 6, the R^2 value is 0.9977, indicating a good degree of fit.

Table 2. Coefficient fitting values of $k_0(t)$.

Coefficients	Fitting Values
w_0	0.66
w_1	7.21
w_2	−52.36
w_3	216.24
w_4	−501.12
w_5	599.22
w_6	−286.49

The armature velocity prediction functions combined with Equations (21)–(23) are defined as follows.

$$\begin{cases} v = k_0 v_0 \\ k_0 = k_0(t) \cdot \left[r_1 \ln(\sigma_d) + r_2 \ln(\sigma_g) + s_0 \right] \\ k_0(t) = \sum\limits_{i=0}^{6} w_i \, t^i \end{cases} \tag{24}$$

Equation (24) fully considers the influence of dynamic conductivity on the armature velocity, which can predict the value of the armature velocity at any moment and with any cases of conductivity.

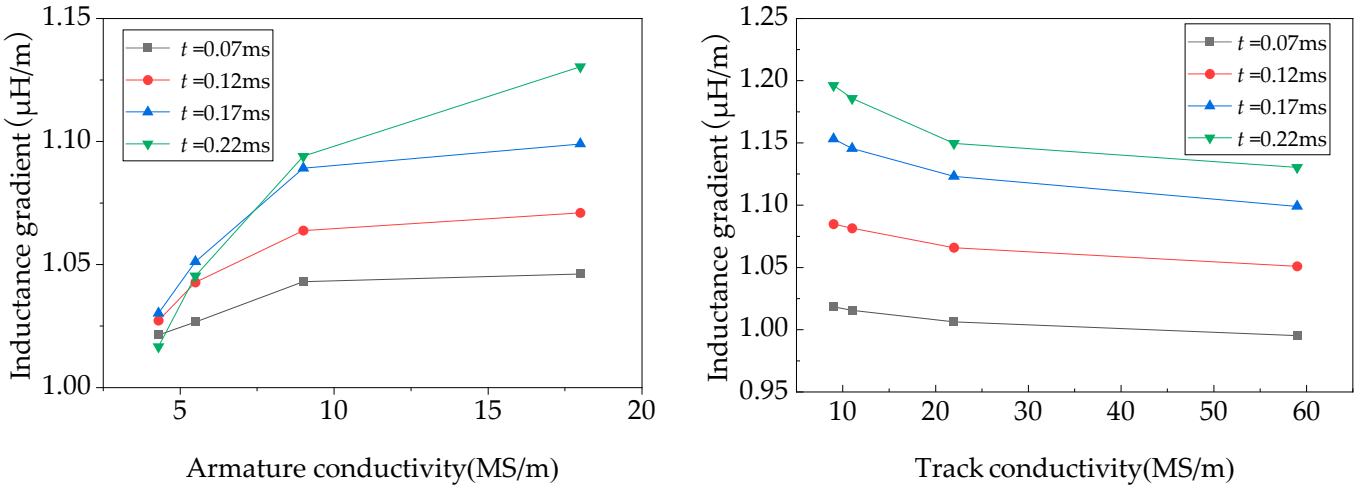
3.2. Prediction Function of Inductance Gradient

According to Figure 8, taking 0~0.24 ms as the rising stage and 0.24~0.6 ms as the declining stage, approximate descriptions of the inductance gradient for the two stages are as follows.

$$\begin{cases} L_{up}(t) = k_1 (k_2 t)^{p_1} + q_1 \\ L_{down}(t) = p_2 t + q_2 \end{cases} \tag{25}$$

where $L_{up}(t)$ is the inductance gradient in the rising stage, $L_{down}(t)$ the inductance gradient in the declining stage and k_1, k_2, p_1, p_2, q_1, q_2 are fitting coefficients.

In the rising stage, the inductance gradient relations with the armature conductivity and track one at different time are obtained, which are shown in Figure 15.

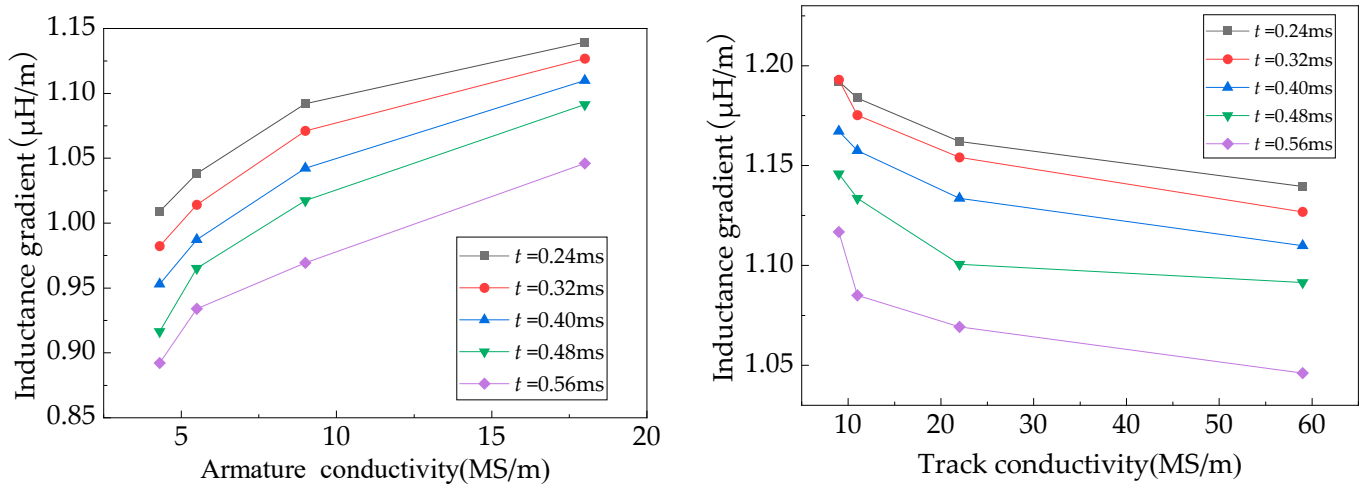


(**a**) (**b**)

Figure 15. The inductance gradient relations with the conductivity at different times in the rising stage. (**a**) Inductance gradient with the armature conductivity σ_d; (**b**) inductance gradient with the track conductivity σ_g.

It can be seen that, in the rising stage, at the same time point, the inductance gradient gradually increases with the armature conductivity σ_d, and gradually decreases with the track conductivity σ_g. Moreover, the ascending (descending) speed gradually slows down.

In the declining stage, the inductance gradient relations with the armature conductivity and track one at different times are obtained, which are shown in Figure 16.



(**a**) (**b**)

Figure 16. The inductance gradient relations with the conductivity at different times in the declining stage. (**a**) Inductance gradient with the armature conductivity σ_d; (**b**) inductance gradient with the track conductivity σ_g.

It can be seen that, in the declining stage, at the same time point, the inductance gradient gradually increases with the armature conductivity σ_d, and gradually decreases with the track conductivity σ_g, in which the ascending (descending) speed gradually slows

down. So, the following equation can be used to approximately describe the inductance gradient with the armature conductivity and track one in the two stages.

$$\begin{cases} L_1 = a_1 \ln(\sigma_d) + b_1 \\ L_2 = a_2 \ln(\sigma_g) + b_2 \\ L_3 = a_3 \ln(\sigma_d) + b_3 \\ L_4 = a_4 \ln(\sigma_g) + b_4 \\ L_5 = a_5 \ln(\sigma_d) + b_5 \\ L_6 = a_6 \ln(\sigma_g) + b_6 \end{cases} \tag{26}$$

where L_1–L_6 are the influence factors of the inductance gradient under the influence of the armature conductivity and the track one, respectively. σ_d and σ_g are the armature conductivity and the track one (MS/m), respectively. a_1–a_6, b_1–b_6 are the corresponding fitting coefficients, respectively.

The inductance gradient prediction functions combined with Equations (25) and (26) are defined as follows.

$$\begin{cases} L_{up} = k_1(k_2 t)^{(a_1 \ln(\sigma_d)+b_1)\cdot(a_2 \ln(\sigma_g)+b_2)} + (a_3 \ln(\sigma_d) + b_3) \cdot (a_4 \ln(\sigma_g) + b_4) \\ L_{down} = p_2 t + a_5 \ln(\sigma_d) + a_6 \ln(\sigma_g) + b_0 \end{cases} \tag{27}$$

where, $b_0 = b_1 + b_2$.

Equation (27) fully considers the influence of the dynamic conductivity on the inductance gradient, which can predict the value of the inductance gradient at any moment and with any cases of conductivity.

3.3. Parameter Identification and Verification of Improved Model

The improved model is based on the simultaneous solution of Equations (24) and (27). According to the improved model, the armature velocity and inductance gradient can be considered as a ternary function related to armature conductivity σ_d, track conductivity σ_g and time t.

In order to make the prediction results of the improved model effective, the error between the predicted value of the improved model and the finite element calculated value should be as small as possible when the conductivity and time are the same. The average relative error is defined as follows:

$$\begin{cases} e_v = \frac{1}{M} \cdot \frac{1}{N} \cdot \frac{1}{T} \sum_{i=0}^{M} \sum_{j=0}^{N} \sum_{k=0}^{T} \left| \frac{v_{i,j,k} - v'_{i,j,k}}{v'_{i,j,k}} \right| \\ e_L = \frac{1}{M} \cdot \frac{1}{N} \cdot \frac{1}{T} \sum_{i=0}^{M} \sum_{j=0}^{N} \sum_{k=0}^{T} \left| \frac{L_{i,j,k} - L'_{i,j,k}}{L'_{i,j,k}} \right| \end{cases} \tag{28}$$

where e_v is the average relative error of the armature velocity, e_L the average relative error of the inductance gradient, M the group number of the finite element calculations of the armature conductivity σ_d, N the group number of the finite element calculations of the track conductivity σ_g, T the number of time points, $v_{i,j,k}$, $L_{i,j,k}$ the improved model predicted values of the armature velocity and inductance gradient, respectively, $v'_{i,j,k}$, $L'_{i,j,k}$, the finite element calculated values of the armature velocity and inductance gradient, respectively.

The armature acceleration can be obtained by differentiating the armature velocity, namely:

$$a_v(\sigma_d(t), \sigma_g(t), t) = \frac{dv(\sigma_d(t), \sigma_g(t), t)}{dt} \tag{29}$$

In addition, the armature acceleration can also be obtained by Equation (15) as follows:

$$a_L(\sigma_d(t), \sigma_g(t), t) = \frac{I^2(t)}{2m_0} \cdot L(\sigma_d(t), \sigma_g(t), t) \tag{30}$$

Discretizing Equation (30):

$$\begin{cases} a_v(\sigma_d(k+1),\sigma_g(k+1),k+1) \\ = \frac{v(\sigma_d(k+1),\sigma_g(k+1),k+1)-v(\sigma_d(k),\sigma_g(k),k)}{\Delta t} \\ a_L(\sigma_d(k+1),\sigma_g(k+1),k+1) \\ = \frac{I^2(k+1)}{2m_0}L(\sigma_d(k+1),\sigma_g(k+1),k+1) \end{cases} \tag{31}$$

According to Equation (31), e_a is defined as follows:

$$e_a = \frac{1}{T}\sum_{k=0}^{T}\left|\frac{a_v(\sigma_d(k),\sigma_g(k),k) - a_L(\sigma_d(k),\sigma_g(k),k)}{a_v(\sigma_d(k),\sigma_g(k),k)}\right| \tag{32}$$

e_v, e_L, e_a are regarded as the objective functions, and the parameters of the improved model are identified to make the objective functions minimum. Considering that the objective functions contain a first-order differential term and are nonlinear, the general identification method easily falls into the local optimal. Therefore, this paper improves on the basis of the particle swarm optimization algorithm, selects the optimal individual for each iteration through the gene sequence crossover and mutation of the genetic algorithm and saves the information and the PSO-GA hybrid algorithm is obtained, which is suitable for solving optimization problems with nonlinear high-dimensional functions, global convergence is good and it can effectively solve the problem of a population falling into the local optimal due to the calculated stability. The specific process is shown in Figure 17:

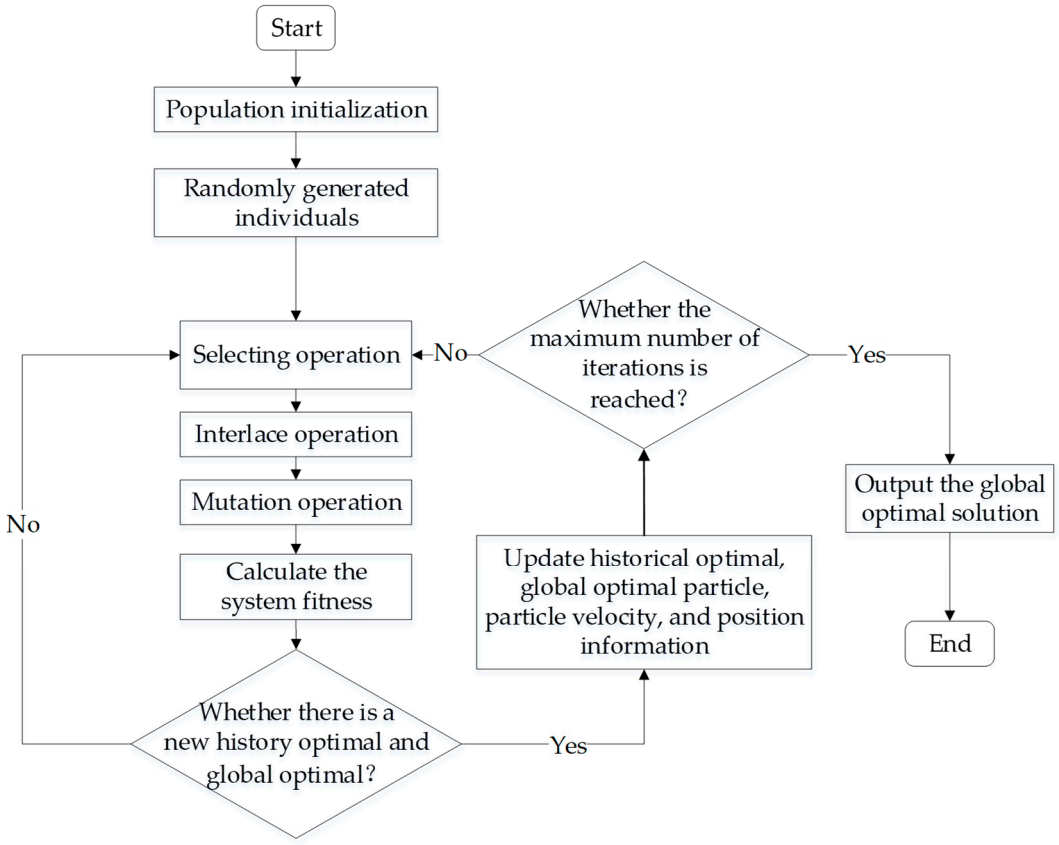


Figure 17. Proposed PSO-GA hybrid algorithm.

The specific computational steps of the algorithm are as follows:

First, population initialization is performed and random individuals are generated, then, the gene editing part of the GA is run, which specifically includes:

(1) Selection operation

According to the size of the fitness to select the better individuals to form a new population; the larger the fitness value, the higher the probability of being selected.

(2) Crossover operation

This refers to the genetic exchange of any two individuals in the population to form new individuals.

(3) Mutation operation

An individual is selected with a certain probability of carrying out one or more gene mutations and produce a new individual after the mutation.

Next, it is determined whether a solution superior to the current population is produced, and if so, it is recorded. If not, the GA algorithm is rerun to obtain a better solution.

After generating a better solution, the PSO algorithm section is run to record the local and global optimal solutions under the current iteration and then updates the velocity and position information of the current particles based on the above solutions, which ensures that the particles move in the optimal direction. After this, the particle information and iteration information are recorded. Moreover, the next generation of iterations is performed.

The calculated parameter identification values of the improved model are obtained by the algorithm as shown in Table 3:

Table 3. Parameter identification values of the improved model.

Parameters	Identification Values	Parameters	Identification Values
r_1	0.0550	a_5	−0.2760
r_2	−0.0300	a_6	0.0968
s_0	0.9641	b_0	1.0034
k_1	2.0023	b_1	−0.1835
k_2	0.5013	b_2	0.7222
a_1	0.1350	b_3	−0.7680
a_2	−0.0710	b_4	0.6185
a_3	0.1702	q_2	−0.0158
a_4	0.2900		

To verify the established improved model, another ten sets of finite element calculated values are taken and compared with the predicted values of the improve model, and the relative error can be calculated by Equation (33).

$$\begin{cases} e_{rv} = \left| \frac{v_f - v_p}{v_f} \right| \\ e_{rL} = \left| \frac{L_f - L_p}{L_f} \right| \end{cases} \tag{33}$$

where, v_f, L_f are the finite element calculated values, v_p, L_p the predicted values of improve model, e_{rv} the relative error between v_f and v_p, e_{rL} the relative error between v_f and v_p.

The relative error is calculated as shown in Tables 4 and 5:

Table 4. Relative error analysis of the armature velocity.

Number	Finite Element Calculated Values (v_f)/(m/s)	Predicted Values of Improved Model (v_p)/(m/s)	Relative Error (e_{rv})/(%)
1	921.63	905.04	1.80
2	1835.66	1851.38	0.86
3	1943.88	1932.96	0.56
4	2011.34	2035.08	1.18
5	2249.60	2222.86	1.19

Table 5. Relative error analysis of the inductance gradient.

Number	Finite Element Calculated Values (L_f)/(μH/m)	Predicted Values of Improved Model (L_p)/(μH/m)	Relative Error (e_{rL})/(%)
1	0.9951	0.9867	0.84
2	1.0010	1.0137	1.27
3	1.0247	1.0050	1.92
4	1.0454	1.0546	0.87
5	1.1799	1.1708	0.77

It can be seen that e_{rv} and e_{rL} are controlled to within 3%. Therefore, it can be considered that the improved model established in this paper can accurately predict the armature velocity and inductance gradient.

4. Experimental Verification

In order to further verify the validity of the improved model, an electromagnetic track launcher experimental platform is built for this research, whose working principle is as follows: the pulsed power supply is charged by a battery charger, which generates an excitation current and causes the armature to launch.

The light curtain device is used to measure the armature velocity in this paper, the schematic diagram of the device is shown in Figure 18.

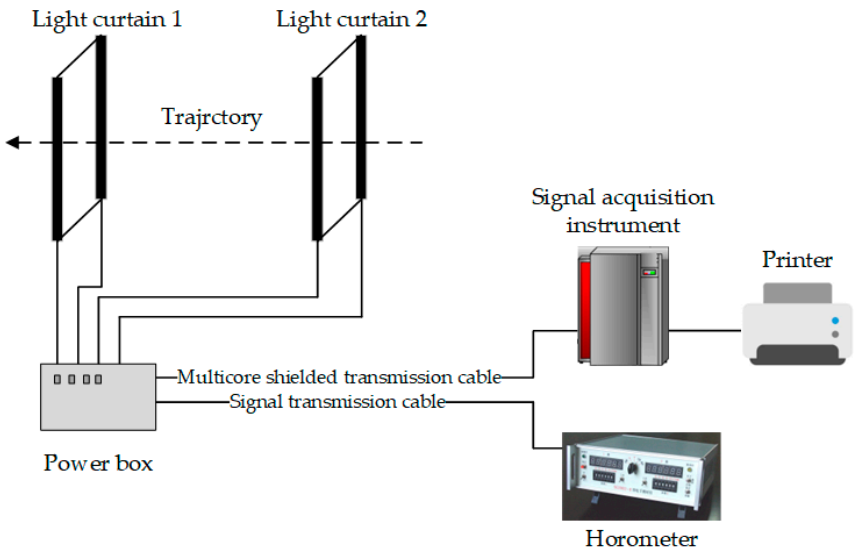


Figure 18. Schematic diagram of the light curtain device.

When the armature passes through the light curtain at a high speed, two light curtains record the armature passing time; the distance of the light curtain handle is fixed at 550 mm, and the armature velocity can be calculated by reading the time difference between the armature passing through the two light curtain.

An XGK-2002 type light curtain is used in this experiment, which has the advantages of high sensitivity, not being affected by ambient light and it can test high-speed objects, etc. Its technical indicators are shown in Table 6.

Table 6. The technical indicators of the light curtain.

Technical Indicators	Values
Range of speed measurement	20–3000 m/s
Relative error of measurement	no greater than 0.1%
Temperature of environment	−10–50 °C
Power supply	AC220 V 50/60 Hz
Power	0.5 A 220 V mean power 60 W

The electromagnetic track launcher experimental platform is shown in Figure 19.

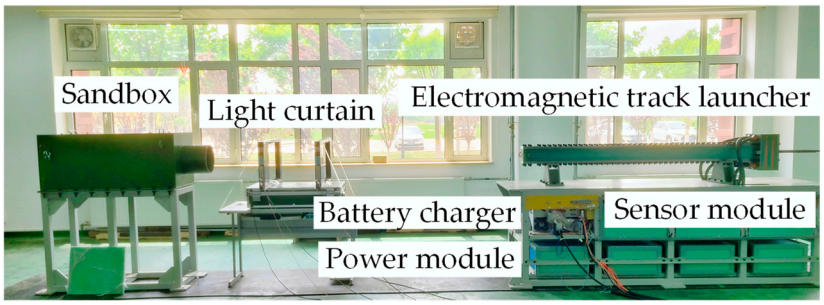


Figure 19. Electromagnetic track launcher experiment platform.

Where the sensor module is mainly used to collect experimental data, the power module and battery charger provide an excitation current for the armature, the light curtain is used to measure the armature velocity and the sandbox is used to receive the armature.

The armature velocity under actual conditions is obtained by the experimental platform, and compared with the calculated value by Ls-dyna and the predicted value of the improved model, the relative error can be calculated according to Equation (34).

$$\begin{cases} e_{\mathrm{rs}} = \left| \frac{v_{\mathrm{e}} - v_{\mathrm{s}}}{v_{\mathrm{e}}} \right| \\ e_{\mathrm{rm}} = \left| \frac{v_{\mathrm{e}} - v_{\mathrm{m}}}{v_{\mathrm{e}}} \right| \end{cases} \tag{34}$$

where v_{e} is the experimental test value, v_s the calculated values by Ls-dyna and v_m the predicted values of the improve model. e_{rs} is the relative error between v_{e} and v_{s}, and e_{rm} the relative error between v_{e} and v_{m}.

The relative errors are calculated as shown in Table 7.

Table 7. Error comparison between v_{e} with v_{s} and v_{m}.

Type	Value/(m/s)	Relative Error/(%)
Experimental test value (v_{e})	2295.45 ± 2.95	-
Calculated value by Ls-dyna (v_{s})	2428.41	5.79 ± 0.13 (e_{rs})
Predicted value of improved model (v_{m})	2322.53	1.18 ± 0.13 (e_{rm})

It can be seen that e_{rm} is reduced by 4.61% compared with e_{rs}, which is closer to the actual launch situation, further proving the validity of the improved model. In conclusion, it can be considered that the improved model in this paper can predict the output under the actual working process more accurately, which provides a certain theoretical basis for the full true simulation of electromagnetic track launch.

5. Conclusions

(1) The finite element analysis for the electromagnetic-thermal field is carried out to obtain the distribution of the temperature and current density, which provides a theoretical basis for the numerical calculation of electromagnetic track launch.

(2) This paper mainly studies the armature velocity and inductance gradient variation rules of the electromagnetic track launcher under the influence of a dynamic conductivity. When the track conductivity is fixed, the armature velocity and inductance gradient increase gradually with the armature conductivity. When the armature conductivity is fixed, the armature velocity and inductance gradient decrease gradually with the track conductivity.

(3) According to variation rules of the armature velocity and inductance gradient, the improved electromagnetic-thermal coupling model of the electromagnetic track launcher considering dynamic conductivity is established. The proposed PSO-GA hybrid algorithm is used to identify the parameters of the established model. Moreover, another ten sets of finite element calculated values are taken and compared with the predicted values of the improved model, whose relative error is controlled to within 3%. The validity of the improved model is verified.

(4) An experimental platform is built to further verify the improved model. Compared with the available finite element calculation, the proposed model in this paper has a smaller error, which is closer to the experimental test value, which is reduced by 4.61% Thus, it can provide a certain theoretical basis for the study of the dynamic parameters of electromagnetic track launch.

Author Contributions: Conceptualization, R.Y. and J.J.; methodology, R.Y. and J.J.; software, J.J. and K.A.; validation, J.J.; formal analysis, R.Y. and J.J.; investigation, R.Y., J.J. and K.A.; resources, R.Y. and K.A.; data curation, R.Y. and J.J.; writing—original draft preparation, R.Y. and J.J.; writing—review and editing, R.Y. and J.J.; visualization, J.J.; supervision, Q.Y. and R.Y.; project administration, Q.Y. and R.Y.; funding acquisition, Q.Y. and R.Y. All authors have read and agreed to the published version of the manuscript.

Funding: This research was funded by the Major Research Program of the National Natural Science Foundation of China, grant number 92066206, S&T Program of Hebei, grant number 215676146H, and S&T Program of Hebei, grant number 225676163GH.

Institutional Review Board Statement: Not applicable.

Informed Consent Statement: Not applicable.

Data Availability Statement: All data, models generated or used during the study appear in the submitted article.

Conflicts of Interest: The authors declare no conflict of interest.

References

1. Ma, W.; Lu, J.; Li, X. Electromagnetic launch ultra-high speed integrated projectile. *J. Natl. Univ. Def. Technol.* **2019**, *41*, 1–10.
2. Lu, J.; Feng, J.; Li, K.; Li, L. Review on guided hypervelocity projectiles. *J. Harbin Eng. Univ.* **2021**, *42*, 1418–1427.
3. Ma, W.; Lu, J. Electromagnetic launch technology. *J. Natl. Univ. Def. Technol.* **2016**, *38*, 1–5.
4. Du, P.; Lu, J.; Feng, J.; Tan, S.; Li, K.; Li, X. Numerical Simulation of Dynamic Launching Process of Electromagnetic Rail Launcher with Electromagnetic and Structural Coupling. *Trans. China Electrotech. Soc.* **2020**, *35*, 3802–3810.
5. Zhang, Y.; Lu, J.; Tan, S.; Wu, H.; Li, B.; Jiang, Y. Analysis of dynamic response characteristics of interior ballistics process in electromagnetic rail launcher. *J. Natl. Univ. Def. Technol.* **2019**, *41*, 18–24.
6. Lin, Q.; Li, B. Modeling and Simulation of Electromagnetic Railgun Launching Process Based on a Transient Multi-physical Field Solver. *Acta Armamentarii* **2020**, *41*, 1697–1707.
7. Lu, J.; Du, P.; Feng, J.; Tan, S. Simulation Study on Critical Velocity of Electromagnetic Rail Launcher. *Proc. CSEE* **2019**, *39*, 1862–1870.
8. Nie, J.; Han, J.; Jiao, Q.; Jin, Z.; Zhang, F. Effect of Rail type Electromagnetic Launcher Dimensions on Inductance Gradient. *High Voltage Eng.* **2010**, *36*, 728–732.
9. Batteh, J. Momentum equation for arc-driven rail guns. *J. Appl. Phys.* **1984**, *56*, 3182–3186. [CrossRef]
10. Yang, Y.; Wang, J.; Xue, W. Simulation and Analysis for Dynamic Load Characteristic of Rail-gun. *Acta Armamentarii* **2010**, *31*, 1026–1031.
11. Zhai, X.; Li, X.; Liu, H.; Peng, Z. Analysis of dynamic inductance gradient of electromagnetic rail launcher. *J. Natl. Univ. Def. Technol.* **2022**, *44*, 156–163.

12. Peng, Z.; Wang, G.; Zhai, X.; Zhang, X. Modeling and Analysis of Time-Varying Inductance Gradient for Electromagnetic Rail Launcher. *Trans. China Electrotech. Soc.* **2020**, *35*, 4843–4851.
13. Wang, Z.; Yuan, W.; Yan, P. Inductance Gradient for Rail-type Electromagnetic Launcher Under Transient Conditions. *High Voltage Eng.* **2017**, *43*, 4039–4044.
14. Ruan, J. *Numerical Calculation and Application of Vortex Field in Moving Conductors*; Science Press: Beijing, China, 2019.
15. Fan, W.; Su, Z.; Zhang, T.; Liu, Y.; Guo, W.; Jin, W. Spatial-temporal Distribution of Transient Temperature Rise in Augmented Electromagnetic Railgun. *High Voltage Eng.* **2021**, *47*, 3346–3354.
16. Lin, L.; Zhao, Y.; Yuan, W.; Yan, P. Thermal Effect Analysis of Railgun Tests Under Transient Conditions. *High Voltage Eng.* **2016**, *42*, 2864–2869.
17. Lin, Q.; Li, B. Measurement and numerical simulation of transient electromagnetic field in railgun. *Acta Armamentarii* **2016**, *37*, 1788–1794.
18. Nong, A.; Ma, S.; Yang, F.; Ma, H.; Ma, D. Calculation of heat production in rail during electromagnetic gun firing by analytical method. *Ordnance Mater. Sci. Eng.* **2022**, *45*, 17–25.

Disclaimer/Publisher's Note: The statements, opinions and data contained in all publications are solely those of the individual author(s) and contributor(s) and not of MDPI and/or the editor(s). MDPI and/or the editor(s) disclaim responsibility for any injury to people or property resulting from any ideas, methods, instructions or products referred to in the content.